Numerical simulation of aeroacoustic sound generated by a simplified side mirror model

Simulation numérique de bruit aéroacoustique engendré par un modèle simplifié de rétroviseur extérieur

R. Siegert,
Daimler Chrysler Research and Technology,
D-70546 Stuttgart,
Tel.: +49 711-17 21724,
Fax: +49 711-17 5834,
e-mail : raimund.siegert@daimierchrysler.com

The work presented here is aiming at a numerical study of noise generation mechanisms due to flow over car side mirrors. For that purpose, the simulation tools have been applied to a generic body representing the major features of the real case flow structures. In a first step, the unsteady flow has been solved using the code Star-CD yielding the unsteady surface pressure distribution. In a second step, this surface pressure source strengths are used as to predict the far-field radiated sound signals. The results from both steps are compared to results of wind tunnel experiments.

L'étude présentée ici est dédiée à l'analyse numérique des mécanismes de génération de bruit dû à l'écoulement autour de rétroviseurs extérieurs automobiles. Dans cette optique, les outils de simulation numérique sont validés sur une géométrie simplifiée. Dans un premier temps, l'écoulement instationnaire est simulé en utilisant le logiciel Star CD. Les distributions de pression pariétale instationnaires ainsi calculées constituent les débits de source acoustiques. Dans un deuxième temps, le rayonnement acoustique, dû à ces sources de caractéristique dipolaire est calculé grâce à un logiciel de prévision de bruit basé sur l'analogie aéroacoustique. Afin de valider les résultats des simulations aérodynamique et aéroacoustique, une expérience dans la soufflerie anéchoïque du FKFS à Stuttgart a été menée. Ces données de mesures sont ensuite confrontées aux résultats de simulation.

Introduction

Due to recent progress in reduction of motor and tire noise, the aerodynamic noise has become a major noise source in acoustic car design [1,2]. Besides the reduction of overall noise levels, the impact of geometric changes on the subjective noise perception is becoming more and more important. Single tones or narrow bands emerging from a spectrum generated by vortex separations on side mirrors are generally very annoying.

Due to shortening product development cycles, reliable simulation tools for noise predictions are becoming more and more important. A validation of simulation tools requires a definite experimental configuration. In the real side mirror case the influence of secondary noise sources such as wheel housing, wiper bay and A-pillar are difficult to separate from the primary noise radiation due to the flow over a side mirror. Therefore a generic model (fig. 1) has been defined to study the noise generation mechanisms.

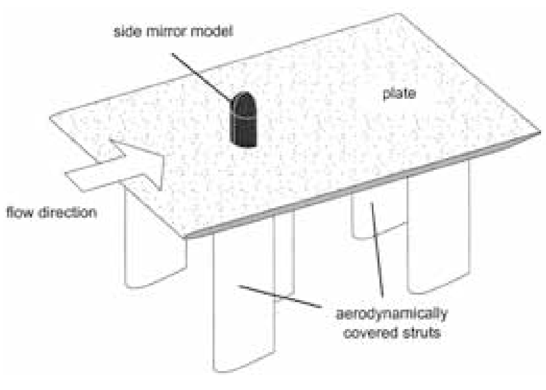

Fig. 1: Experimental setup of the side mirror model

Experimental set-up

This test case has the shape of a simplified external car mirror mounted on a flat plate. The mirror is defined by a half-cylinder with 0,2 m diameter and length, blunted by a quarter of a sphere with the same diameter. The mirror is mounted on a flat plate with 1,6 m width and 2,4 m length. Fig. 1 shows a sketch of the experimental setup. The plate was used in order to guarantee clearly defined boundary conditions around the mirror.

The mirror model was mounted 0,9 m downstream of the elliptically shaped leading edge of the flat plate. Both side edges of the plate with 0,05 m strength were rounded and the sharp trailing edge was formed wavy to prevent the

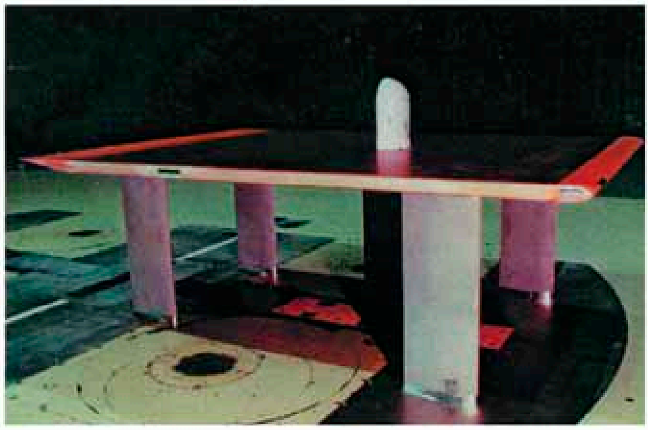

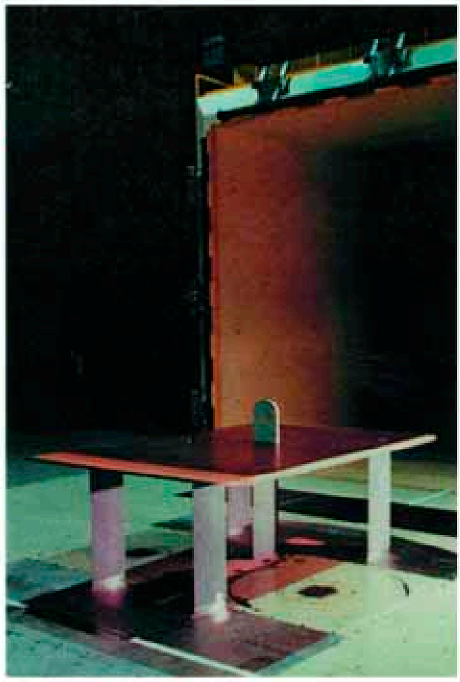

Fig. 2: Experimental set-up in the aeroacoustic wind tunnel FKFS at Stuttgart

separation of coherent wake structures. The flat plate was mounted on 4 struts with 0,8 m length and 0,15 m chord length. The struts were streamlined using a NACA0015 profile. The setup was completed by an additional hollow strut of same dimensions, mounted under the mirror and covering pressure tubes and electrical cables for various measurements. Fig 2 shows the experimental setup in the FKFS-aeroacoustic [3] wind tunnel at the University of Stuttgart.

For comparisons with the numerical approach the steady surface pressure distribution as well as transient pressure/time histories have been measured at selected positions on the mirror as well as on the plate (fig. 3).

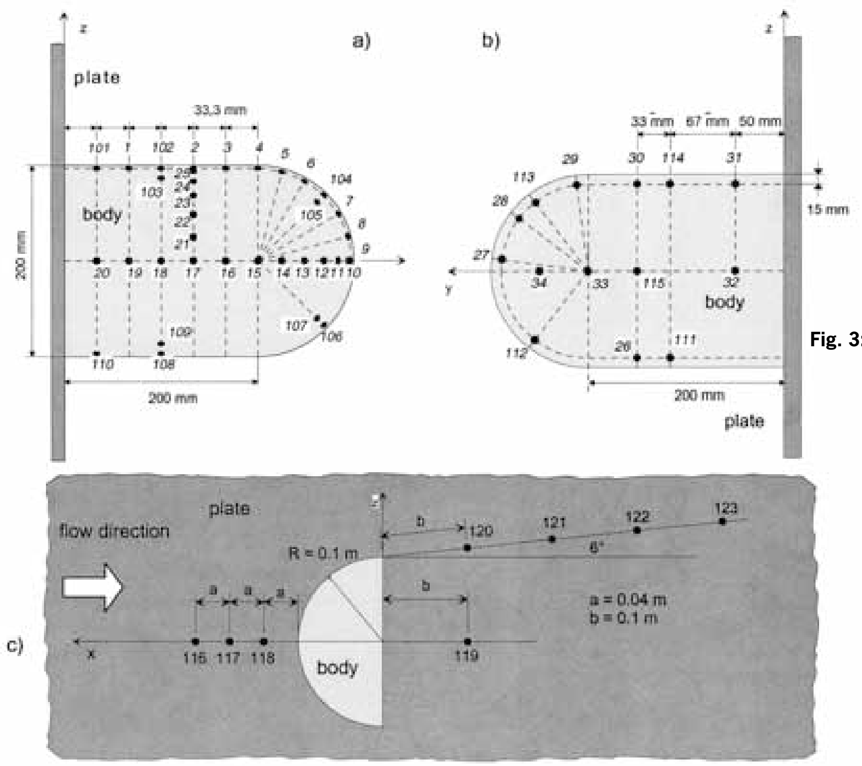

Fig. 3: Locations of the surface pressure probes. Front view (a), rear view (b) and top view (c).

Time averaging, steady state transducers (no. 1-34) and transient relativ pressure tranducers (no. 101-123).

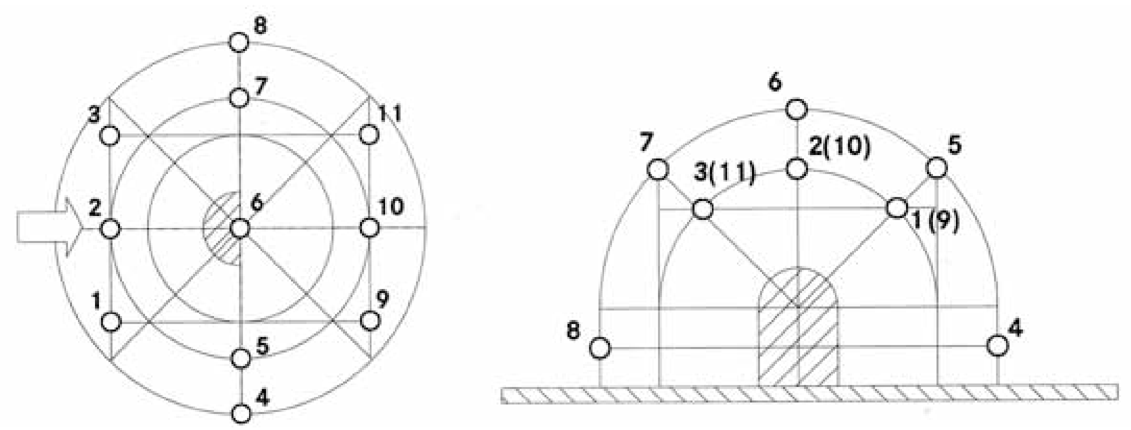

Fig. 4: Microphone positions for inflow acoustic measurements
(a) top view and
(b) front view

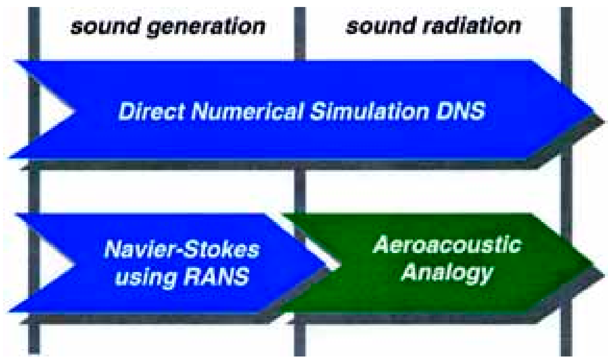

Figure 5: Numerical approaches to aeroacoustic problems

Besides the unsteady surface pressures, the sound radiation has been measured using an inflow microphone. Figure 4 shows the 11 microphone positions placed on an envelope about 0.5 m from the body. These positions have been chosen outside the direct upstream and downstream area of the body to prevent wake flow interactions in both cases.

Numerical approach

In low Mach number flows Ma<0.4 the dominant acoustic source is known to be the unsteady surface pressure distribution with dipolar radiation characteristic. The relevant sources are therefore comprised in regions with high unsteady surface pressure amplitudes as in the case of flow separations or wake/wall interactions.

Aeroacoustic simulation

Basically there exist two approaches to predict the radiated sound generated aerodynamically. The first approach consists in a one-step, direct simulation of sound generation and propagation. The advantage of this approach resides in the numerical resolution of all relevant vortex scales.

The resolution of aeroacoustic pressure fluctuations (less than 1 Pa) and their propagation at all relevant wave lengths (less than 0.1 m) requires :

(i) very high spatial and temporal resolution in a huge calculation domain and
(ii) very accurate high order numerical codes. The numerical expenditure is therefore extremely high and can currently be carried out only for rather academic problems on high performance computers.

The second approach consists in a separation of the noise generation and propagation problem. This classical aeroacoustic analogy approach has been applied since the early 1950's in the aerospace industry and is based on the work of Lighthill [4], Curle [5] and Ffowcs-Williams and Hawkings [6].

In a first step, the unsteady fluid flow is solved locally using a suitable CFD code. The resulting unsteady surface pressure fluctuations (fig. 6) constitute source strengths used as input for an inhomogeneous wave equation. The advantage of this approach is the use of a suitable mesh for the CFD simulation of the flow field (with local refinements to account for viscous effects) without any restrictions due to the propagation problem (group velocity etc.).

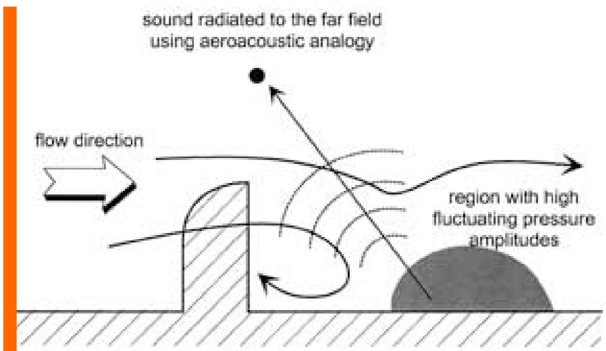

Fig. 6: Schematic representation of the aeroacoustic analogy approach

Unsteady flow simulation

The numerical simulation of the unsteady flow problem has been carried out using the commercialized software STAR-CD [7]. This CFD-code operates by solving the governing differential equations of the flow physics by numerical means for a wide range of applications such as external aerodynamics, engine cooling systems, engine combustion or passenger comfort. Therefore STAR-CD has become the standard CFD-code in automotive industry.

The Reynolds averaged Navier-Stokes equations are discretized by the finite-volume method. Thus, they are first integrated over the individual computational cells, and over a finite time increment and then approximated in terms of the cell-centered nodal values of the dependent variables. This approach has the merit amongst others, of ensuring that the discretized forms preserve the conservation properties of the parent differential equations. The implicit discretization scheme used for the present work is first order accurate in time and second order accurate in space.

STAR-CD employs mathematical models of turbulence to determine the Reynolds stresses and turbulent scalar fluxes. These models comprise additional differential or algebraîc equations that relate the aforementioned unknowns to selected ensemble-averaged properties of the turbulence field and also provide a framework for calculating these properties. In the frame of the present work different turbulence models have tested and a detailed analysis of the solution dependence from spatial and temporal resolution have been carried out.

Aeroacoustic Analogy

Equation (1) represents the inhomogeneous wave equation following Ffowcs-Wiiilams and Hawkings [6], which is derived from the basic fluid dynamic equations using generalized functions [8]. Here the function *f =0*, mathematically describes the surface of the body. The expression on the left hand side of (1) is the wave equation with inhomogeneous source terms on the right hand side.

$$\left(\frac{1}{c_0^2}\frac{\partial^2}{\partial t^2}-\frac{\partial^2}{\partial x_i^2}\right)p' = \frac{\partial}{\partial t}\left[\rho v_n \delta(f)\nabla f\right] - \frac{\partial}{\partial x_i}\left[n_i p \delta(f)\nabla f\right] + \frac{\partial^2}{\partial x_i \partial x_j}\left[T_{ij} H(f)\right] \quad (1)$$

where:

p' = sound pressure [Pa]
r = air density [kg/m3]
n_j = surface normal [-]
c_0 = speed of sound [m/s]
v_n = normal surface velocity [m/s]
p = static pressure [Pa]

$T_{ij} = \rho u_i u_j + p_{ij} - c_0^2 \rho \delta_{ij}$ = Lighthill Tensor [Pa]

δ(f) = Dirac distribution, only defined on the body's surface *f = 0*
H(f) = Heaviside distribution, only defined in the fluid f> 0

The first term on the right hand side represents volume sources (monopole sources of order 0) and describes the displacement effect due to a moving body. The second term comprises so-called force or momentum sources (dipoles, order 1), describing the energy transformation of a fluctuating surface force into sound radiation. The third term stands for vortex or turbulence sources (quadrupole sources, order 2), resulting from turbulent shear stresses.

Even though usually several source types are present simultaneously in any real aeroacoustic problem the source of highest acoustic effficiency will be dominating. The acoustic effficiency η_{ak} 3-dimensional sound radiation depends on the Mach number as follows [9] :

Monopole : $\eta_{ak} \propto Ma$

Dipole: $\eta_{ak} \propto Ma^3$

Quadrupole : $\eta_{ak} \propto Ma^5$

In the case of the flow passing the side mirror model the sound radiation is mainly due to the dipolar contribution generated by the unsteady surface loading. After some manipulations of equation (1) and by neglecting the monopolar and quadrupolar terms we finally obtain:

$$p'_d(x_i,t) = \frac{1}{4\pi c_0}\int_S \left[\frac{r_i}{r^2(1-M_r)^2}\left(\frac{\partial}{\partial \tau}\{n_i \cdot p(y_i,\tau)\} + \frac{n_i \cdot p(y_i,\tau)}{1-M_r}\frac{\partial M_r}{\partial \tau}\right)\right] d\sigma \quad (2)$$

where:
x_i = observer point [m]
y_j = surface element [m]
t = reception time [s]
τ = emission time [s]
r = x_i-y_i = acoustic distance [m]
M_r = relative Mach number [-]
p(y_i,τ) = surface pressure time history at τ in y_j [Pa]
p'(x_i,τ) = sound pressure time history at t in x_i [Pa]

The radiated sound pressure can easily be obtained by inserting the time derivation of the simulated surface pressure data in equation (2) and integrating over the surface. The notation [...] requires the evaluation of the bracketed terms at retarded time.

At Daimler Chrysler, two aeroacoustic tools have been developed on different platforms. The first tool called SOPRANOS [10] is an in-house research code. The second tool, called FLOWNOISE, is linked to SYSNOISE allowing to take into account reflecting surfaces using a boundary element method. Since reflecting surfaces are negligible in this test case, there is no need to present both results in this work.

Results

The flow velocity in the case published here is 140 km/h. The Reynolds number with respect to the body's diameter is Re – 5 x 10^5. By a simple Strouhal number estimation (vortex separation due to the Van Karman effect, St = 0,2), the frequency range of the expected tone and its first harmonics will be approximately 30-200 Hz.

The CFD-model comprised 500 000 fluid cells with several embedded refinement zones. The simulation has been carried out several thousand time steps in order to obtain a clean numerical solution before saving 2 048 time steps with a time step size dt = 2,5e-4 s. The expected dominant tone of about 40 Hz is therefore solved with approximately 100 time steps per period, which seems to be suffficient for the purpose of this study.

Vortex Structures

Figure 7 gives an instantaneous representation in two different views of Lambda2 structures [11] which have been calculated using a STAR-CD simulation with RNG turbulence model. Three distinct phenomena can be observed. First of all a rather large scale horseshoe vortex located in the region upstream of the mirror basis. Second rather small scale vortical structures again horseshoe-shaped which are shed from the sharp trailing edge of the mirror model. These vortices are convected, rolling up and finally merging in progressively larger scale structures. Third the impact of this mirror wake due to the strongly 3-dimensional flow passing the body at about 1,5 diameters downstream of the body.

Surface pressure distribution

Figure 8 shows the rms-values (root mean square) of the fluctuating part of the surface pressure distribution:

$$p'_{ms} = \sqrt{\frac{\sum_{n=1}^{N} p_n(x_i, t_n) - \overline{p}(x_i)^2}{N}} \tag{3}$$

where:
p_n = static pressure at time t_n in point x_i on the surface

$\overline{p}$ = time averaged surface pressure at point x

N = number of time steps

The p'_{ms} values are represented in decibel with pref = 2e-5 Pa. The dark gray regions indicate high pressure fluctuation levels which constitute the relevant dipolar source regions. The most important features are the two lobes of high fluctuation levels on the plate downstream of both vertical trailing edges of the body. They correspond to the passing shear layer with vortices rolling up and merging progressively.

Figure 9 shows a comparison between the simulated and measured spectra at two sensor locations (cf. fig. 8 and fig. 3). In the region with high fluctuating level (point 123), a good agreement is found below 100 Hz. Above this frequency, the simulation more and more underestimates the measured spectra. This indicates, that the temporal resolution of the current STAR-CD simulation is not suffficient.

At the sensor location 103 (fig. 10) the simulated spectrum is about 15 dB below the measured values over the entire frequency range. In this region two phenomena can be observed. First the transition laminar/turbulent transition of the boundary layer and second a local flow separation which can both not be solved correctly using the RNG turbulence model. Fortunately the influence on the overall radiated noise of this region with a strong discrepancy between simulation and measurement is negligible, since the dominant aeroacoustic sources are localized on the plate where the simulated pressure levels are in good agreement with the experiment.

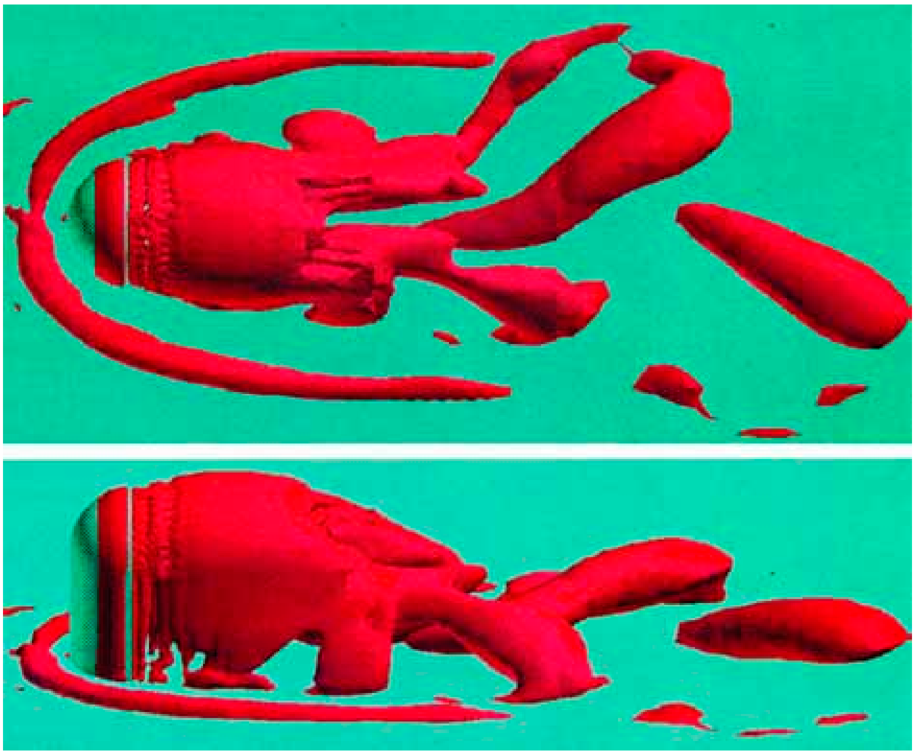

Fig. 7: Top view and side view of Lambda2-Structures in the vicinity of the mirror model

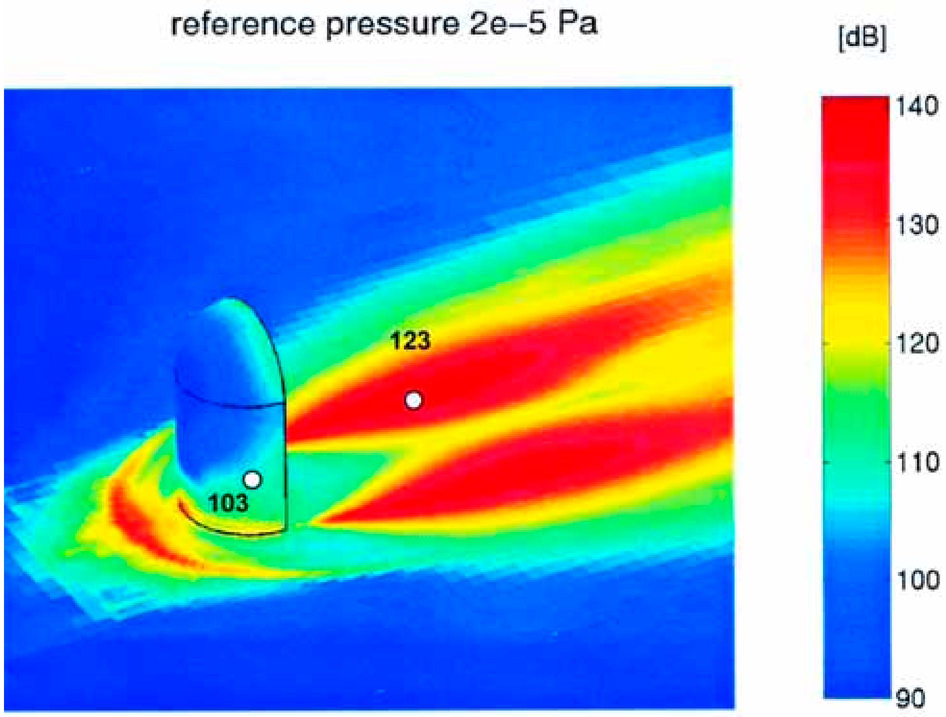

Fig. 8: Simulated pms-distribution of the surface pressure in decibel

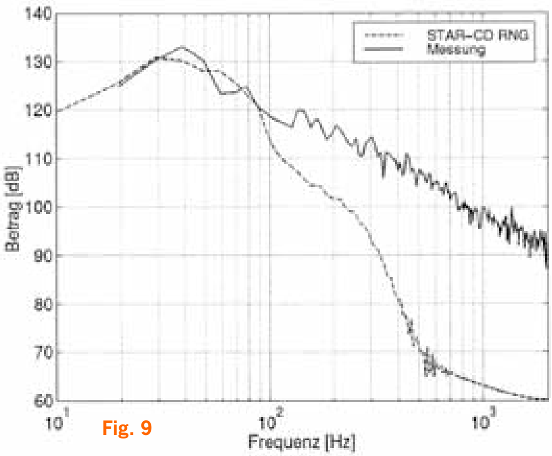

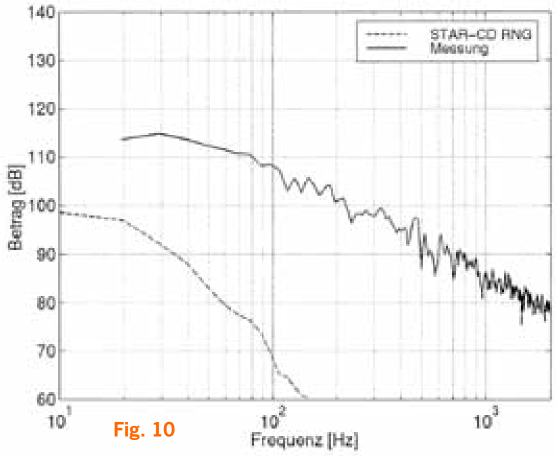

Fig. 9: Comparison simulation/measurement at sensor location 123

Fig. 10: Comparison simulation/measurement at sensor location 103

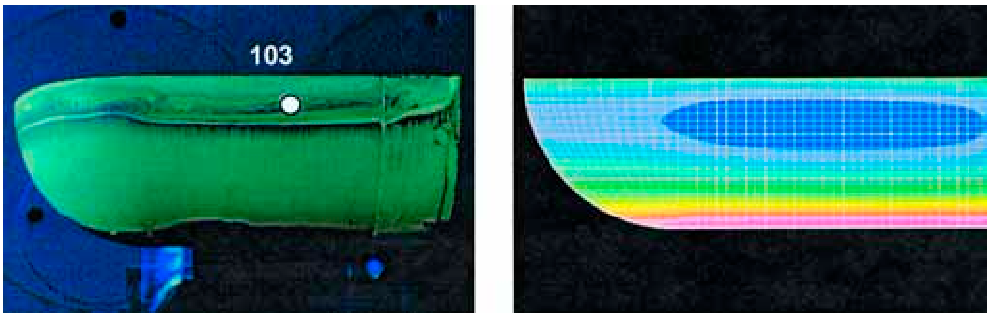

Fig. 11: Flow visualization using oil flow patterns (a) on side mirror body and STAR-CD simulation show separation line upstream of the trailing edge

Time/Frequency Signature

Another interesting feature is the time/frequency signature of the fluctuating pressure signals in the body's wake. As already mentioned above, a discrete tone due to vortex shedding should be dominating the spectra. Unfortunately the spectra (fig. 11 and 12) appear rather smoothed with no discrete frequency emerging from the spectra.

Figures 12 and 13 show short-term Fourier transforms of the measured and simulated surface pressure at sensor location 123. The discrete vortex shedding frequency is now found at about 40 Hz as expected, but clearly shows a time dependency with a period of about 0,2 s. Within one such period the frequency is shifting from about 20 to 60 Hz for about 0,2 s and completely disappears for about 0,05 s. This is probably due to the already mentioned strong 3D interaction of the vortical structures shed from the edges of the body. The simulated pressure signal shows similar patterns even though the overall signal duration, is too small to confirm the periodicity of the time/frequency signature.

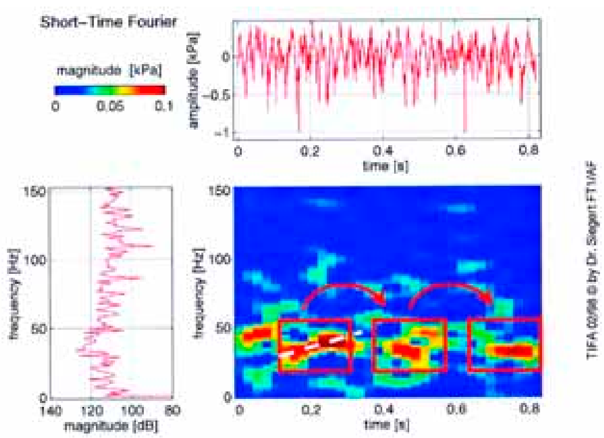

Fig. 12 : Time/frequency analysis of measured surface pressure at sensor 123

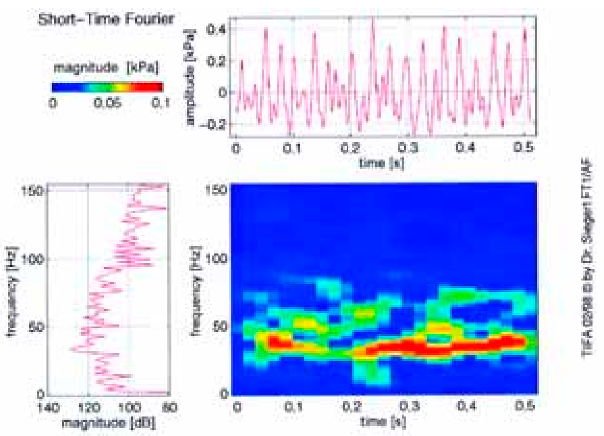

Fig. 13 : Time/frequency analysis of simulated surface pressure at sensor 123

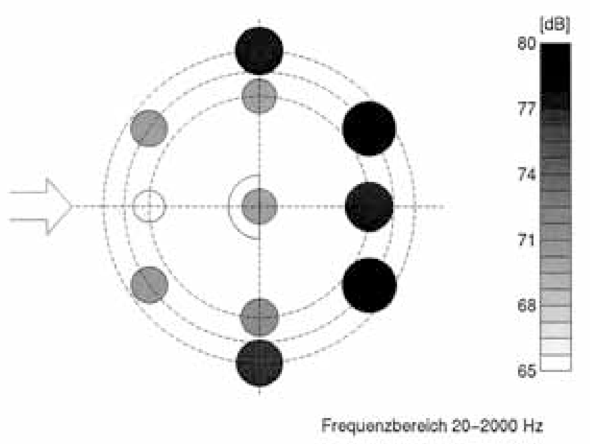

Fig. 14 : Radiation characteristic of the background corrected inflow measurement

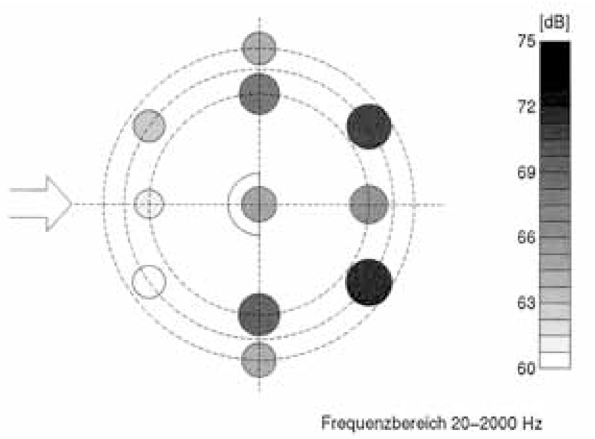

Fig. 15: Radiation characteristic of the aeroacoustic simulation

Acoustic Radiation Characteristic

The comparison between measured and simulated sound signals will be carried out in two ways: (i) the overall noise levels and (ii) the frequency spectra. The frequency range for the integration of noise levels is 20 to 2 000 Hz. The lower frequency limit is due to two facts: (i) the dominant contribution of the background noise in the wind tunnel at frequencies < 20 Hz and (ii) the overall simulated signal period of 0,1 s yielding a sufficient spectral resolution only at frequencies > 10 Hz.

Figures 14 and 15 show a comparison between the simulated and measured overall noise levels for all 11 microphone positions (top view, fig. 3). First of all a good ageement is achieved in terms of radiation characteristic, although the noise levels differ about 2-10 dB depending on the microphone position. The highest noise levels are found at positions 9 and 11 respectively.

A rather big discrepancy is found for positions 4 and 8, which is probably due to the vicinity of the plate side edges.

The noise generated due to the flow passing these edges is not taken into account in the simulation.

Figure 16 shows a comparison between measured and simulated spectra at 4 microphone positions 3,4,6 and 9. First it can be noticed that the simulated acoustic spectra shows the same spectral decay of above 100 Hz as the surface pressure spectra (fig.9 and 10). Below that frequency a mean difference of 2 to 10 dB is found for positions 3 and 6. The aforementioned position 4 shows a 10-15 dB difference.

The relatively big discrepancy at position 9 indicates, that the spatial extend of the region with maximum surface pressure fluctuation levels is not simulated correctly.

The impossibility to separate experimentally the contribution of distinct source regions to the overall noise level can be overcome using aeroacoustic simulation methods. Figure 17 shows the radiation characteristic of the sources located on the mirror body itself. This radiation pattern is in perfect agreement with the typical dipolar radiation field of a vortex shedding cylinder. The maximum sound radiation is perpendicular to the flow direction and normal to the mirror surface whereas the minimum sound is radiated in the vertical direction (position 6).

Conclusions

The purpose of the work presented here was the evaluation of the potential of a numerical tool for the prediction of aerodynamic noise in industrial automotive applications.

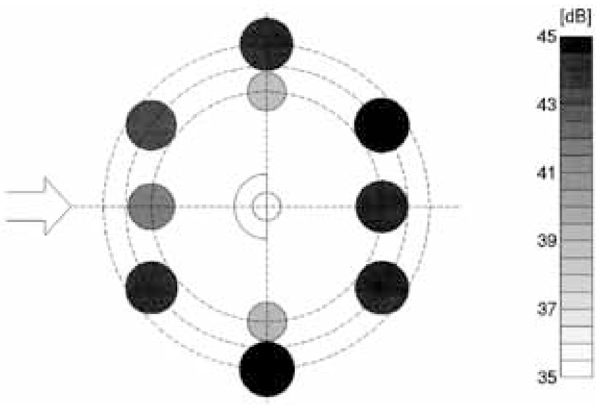

Fig. 17: Radiation characteristic of the sources located on the mirror body

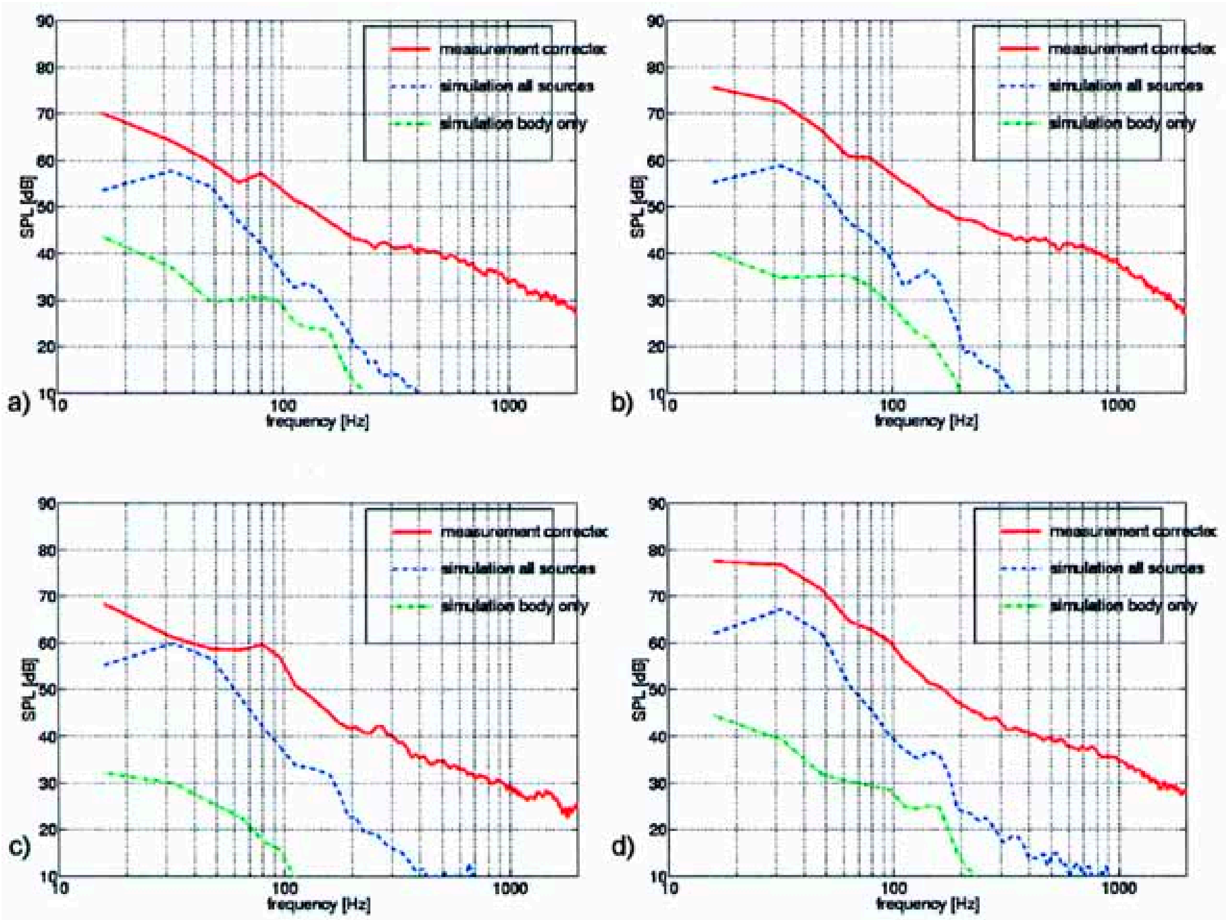

Fig. 16: Comparison of frequency spectra at microphone locations 3 (a), 4 (b), 6 (c) and 9 (d) between simulation and experiment

Therefore simulations have been carried out following a classical aeroacoustic analogy approach. The unsteady surface pressure distributions due to the flow separation at the body and the interaction of the body's wake with the plate have been calculated using the CFD-code STAR-CD.

The sound radiation has been predicted by means of in-house aeroacoustic tools using the unsteady surface pressure distribution as dipolar source strengths. A validation experiment has been carried out in an aeroacoustic wind tunnel both to validate the aerodynamic and the aeroacoustic part of this work.

By analyzing the complex 3D flow structures the understanding of the noise generation mechanisms in the body's wake interacting with the plate have been deepened.

In the body's wake region close to the plate good agreement has been achieved qualitatively and quantitatively below 100 Hz. Especially the time varying behavior of the dominant vortex shedding frequency is in good agreement.

The simulated radiation characteristic has been confirmed by the experimental data yielding a good relative accuracy.

The overall noise levels are underpredicted 2-10 dB, which is not sufficient for real case predictions in industry.

Several important features heve been identified for future applications:

- The surface pressure data has to be written out over longer overall time periods to capture correctly any low frequency behavior of the underlying noise generation mechanisms.

- The time step size should be further reduced in order to increase the upper frequency limit of the simulated spectra.

- Furthermore it must be checked, whether the extend of the region with high fluctuation levels is well represented by the simulations or not.

At the current stage aeroacoustic simulations have proven to be an efficient means to evaluate the integral quality of unsteady CFD-simulations. A particularly interesting feature aeroacoustic simulations offer is the possibility to evaluate the contribution of distinct source regions to the overall noise level.

Acknowledgement

The author is grateful to Daimler Chrysler Car Division and Adtranz Railway Systems for financial and technical support. Any helpful discussions and suggestions from colleagues are also acknowledged.

Bibliography

[1] Ahmed S.R. und 25 Mitautoren, Akustik und Aerodynamik des Kraftfahrzeugs. Grundlagen - Optimierungsmethoden - Me8-und Versuchstechnik., Expert Verlag, ISBN 3-8169-1190-0.

[2] Dobrzynski W., Zur Bedeutung von Stromungswechseldrucken auf der Karosserieoberflache für den Innenlarm von Personenkraftfahrzeugen", DFVLR Forschungsbericht DFVLR-FB 83-28.

[3] Porthoff J., Essers U., Eckoldt D., Fuchs H.V., Der Aeroakustik-Fahrzeugwindkanal der Universität Stuttgart am Institut für Verbrennungsmotoren und Kraftfahrtwesen, Siehe 11, Kapitel 17, PP. 333-373, Expert Verlag, ISBN 3-8169-1190-0.

[4] Lighthill M.J., On sound generated aerodynamically - I. General Theory. Proc. of the Royal Society of London, Series A, Vol. 211, PP. 564-587, 1952.

[5] Curle N., The influence of solid boundaries upon aerodynamic sound. Proc. of the Royal Society of London, Series A, Vol. 231, PP. 505-514, 1955.

[6] Ffowcs-Williams J.E., Hawkings D.L., Sound generated by turbulence and surfaces in arbitrary motion. Phil. Transactions of the Royal Society of London, Series A, Vol. 264, PP. 321-342, mai 1969.

[7] User Guide & Methodology StarCD Version 3.05. Computational Dynamics Limited, 1998.

[8] Jones D.S., Generalized functions, McGraw-Hill Inc, London, 1966.

[9] Grundmann R., Kramer C., Beschreibung von Stromungsgerauschen. Vorlesungsmanuskript, Institut für Industrieaerodynamik FH, Aachen.

[10] Siegert R.U., Bruit engendré par les rotors d'hélicoptères - Etude des mécanismes de génération de bruit et contribution à l'analyse de signaux expérimentaux. Thèse de doctorat, Université Paul Sabatier de Toulouse, 1995.

[11] Jeong J., Hussain F., On the identification of a vortex. J. Fluid Mech., Vol. 285, PP. 69-94, 1995.